Electrochemical behavior of Sn/SnO$_2$ mixtures for use as anode in lithium rechargeable batteries

A. Sivashanmugam [a], T. Prem Kumar [a], N.G. Renganathan [a], S. Gopukumar [a, *],
M. Wohlfahrt-Mehrens [b], J. Garche [b]

[a] *Central Electrochemical Research Institute, Karaikudi 630006, India*
[b] *Center for Solar Energy and Hydrogen Research, Ulm D-89081, Germany*

Abstract

Anodes derived from oxides of tin have, of late, been of considerable interest because, in principle, they can store over twice as much lithium as graphite. A nanometric matrix of Li$_2$O generated in situ by the electrochemical reduction of SnO$_2$ can provide a facile environment for the reversible alloying of lithium with tin to a maximum stoichiometry of Li$_{4.4}$Sn. However, the generation of the matrix leads to a high first-cycle irreversible capacity. With a view to increasing the reversible capacity as well as to reduce the irreversible capacity and capacity fade upon cycling, tin–tin oxide mixtures were investigated. SnO$_2$, synthesized by a chemical precipitation method, was mixed with tin powder at two compositions, viz., 1:2 and 2:1, ball-milled and subjected to cycling studies. A mixture of composition Sn:SnO$_2$ = 1:2 exhibited a specific capacity of 549 mAh g^{-1} (13% higher than that for SnO$_2$) with an irreversible capacity, which was 7% lower than that for SnO$_2$ and a capacity fade of 1.4 mAh g^{-1} cycle^{-1}. Electrodes with this composition also exhibited a coulombic efficiency of 99% in the 40 cycles. It appears that a matrix in which tin can be distributed without aggregation is essential for realizing tin oxide anodes with high cyclability.
© 2005 Elsevier B.V. All rights reserved.

Keywords: Li–Sn alloy anode; Sn–SnO$_2$ mixtures; Capacity fade; Irreversible capacity

1. Introduction

Anodes composed of oxides of tin are of considerable interest because, in principle, they can store over twice as much lithium as graphite [1–3]. During the first charging, tin oxide is reduced to tin, which is dispersed in matrix of lithium oxide [4–7]. The metallic tin may then reversibly react with lithium to form a variety of alloys up to a maximum intake of 4.4 Li per Sn atom to form Li$_{4.4}$Sn [8]. The reactions may be written as:
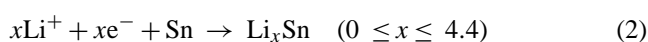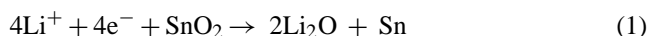
$$4Li^+ + 4e^- + SnO_2 \rightarrow 2Li_2O + Sn \quad (1)$$

$$xLi^+ + xe^- + Sn \rightarrow Li_xSn \quad (0 \leq x \leq 4.4) \quad (2)$$

A nanometric matrix of Li$_2$O generated in situ by the electrochemical reduction of SnO$_2$ can provide a facile environment for the alloying process and facilitate good cycling behavior. However, the generation of the matrix leads to a high first-cycle irreversible capacity. Moreover, the alloying–dealloying reactions are accompanied by large volume changes, which induce mechanical strain resulting in crumbling of the active components upon repeated cycling. Use of tin–tin oxide composites could be a solution in realizing increased reversible capacity as well as reduced irreversible capacity and capacity fade upon cycling, as this could increase the Sn:Li$_2$O ratio in the anode matrix.

Tin dioxide obtained by various synthetic approaches is described in the literature [9–14]. Different textures and microstructures resulting from the various synthesis routes play an important role in the electrochemical behavior of the prod-

* Corresponding author. Fax: +91 4565 227779.
 E-mail address: deepika_41@rediffmail.com (S. Gopukumar).

uct. In this work, we report the results of our studies on the lithium insertion behavior of mixtures of amorphous SnO_2 with tin powder.

2. Experimental

2.1. Active materials

Various synthesis techniques, such as sol–gel [15], chemical vapor deposition [16], magnetron sputtering [17], evaporation of elemental metal tin in an oxidizing atmosphere [18], and ultrasonic spray pyrolysis [19] have been used to prepare SnO_2 powders and films. Here, we have employed a simple precipitation technique for obtaining sub-micron size SnO_2 particles. $SnCl_4$ (Merck) and NH_4OH (Merck) were used as precursors. $SnCl_4$ was dissolved in distilled water. NH_4OH solution was added until the pH value reached 9 upon which a milky white precipitate of $Sn(OH)_4$ formed. The precipitate was filtered and dried in air for a few days. The dehydration process of the gel resulted in SnO_2. The reactions can be expressed as:

$$SnCl_4 + 4NH_4OH \rightarrow Sn(OH)_4 + 4NH_4Cl \qquad (3)$$

$$Sn(OH)_4 \rightarrow SnO_2 + 2H_2O \qquad (4)$$

The dried mass was ground to a fine powder and heat-treated in air for 5 h. The SnO_2 thus prepared was mixed with Sn powder (Merck) in 2:1 and 1:2 proportions and ball-milled for 2 h in a planetary ball mill with 10-mm zirconia balls at a balls-to-mix weight ratio of 9:1. The morphology and structure of the mixtures and the parent materials were examined by scanning electron microscopy (Zeiss, DSM 940) and X-ray diffraction (Siemens, D5000). Galvanostatic cycling studies were carried out on a computerized cycling device (BEATE). Cycling voltammetric studies were performed by a BAS (IM6) electrochemical analyzer (Zahner) at a scan rate of $10\,\mu V\,s^{-1}$. The first scan was run between 3.2 and 0.1 V, while the subsequent ones between 0.1 and 1.0 V versus Li^+/Li.

2.2. Electrochemical cell

A three-electrode glass cell was used for all electrochemical studies. The working electrode was prepared by a slurry coating procedure. A slurry consisting of 85% SnO_2 or Sn or the mixtures, 10% acetylene black as a conducting material and 5% poly(vinylidene fluoride) was prepared in ethyl methyl ketone, and coated over a nickel foam tablet of 1-cm diameter. It was air-dried for a few minutes. The coated foam was enclosed in a Ni mesh packet and pressed under a 10 t load in a hydraulic press for a minute and vacuum-dried overnight at 150 °C. The nickel foam acted as the current collector for the working electrode. Lithium foil (Merck) was used as reference and counter electrodes. The electrolyte was LP 30

(Merck), 1 M solution of $LiPF_6$ in a 1:1 (v/v) mixture of ethylene carbonate and diethyl carbonate. All electrochemical studies were performed in an argon-filled glove box (Mbraun).

3. Results and discussion

3.1. Characterization of Sn, SnO_2 and their mixtures

Fig. 1 shows the XRD pattern of the as-synthesized SnO_2 powder. The peak positions fit well with the standard values of the cassiterite phase of SnO_2 (JCPDS 41-1445). The broad peaks in the XRD pattern suggest that the particles are extremely fine crystallites or are amorphous [20]. Thus, we may say that the precipitation technique, in fact, produced a mixture of amorphous and crystalline particles of SnO_2 of submicron size. A typical SEM image of SnO_2 powder is given in Fig. 2a. It is clear from the image that the powder contained submicron sized particles with good morphology and size control. Moreover, they were in an agglomerated form. Their size varied from about 200 to 300 nm. The SEM image of the Sn powder, given in Fig. 2b, shows that the metal particles were spherical, with tiny particles occupying the voids between the bigger ones. The XRD patterns of the 1:2 and 2:1 mixtures of Sn and SnO_2 are presented in Figs. 3 and 4, respectively. The peaks corresponding to the major constituents in the mixture dominate in the patterns. Furthermore, ball milling did not cause any phase change or introduce any impurity. Typical SEM images of the ball-milled mixtures are given in Fig. 5. The particles appear as agglomerates composed of small units of size 1 μm or less. It is also clear from the images that the milling cleaved the spherical tin particles into some shapeless, burr-like units.

3.2. Cyclic voltammetry of SnO_2

Fig. 6 shows the cyclic voltammograms of SnO_2 for the first four scans. In the first cathodic scan, the peak around 0.9 V is ascribed to the irreversible conversion of SnO_2 to
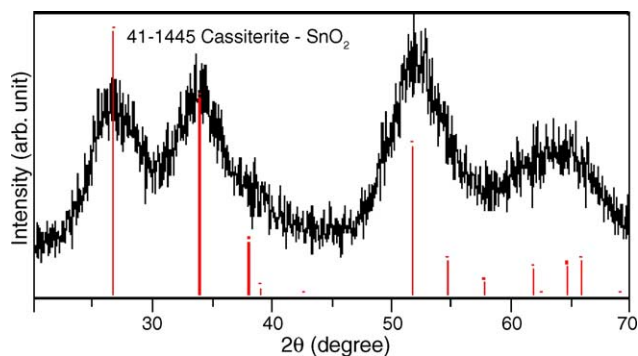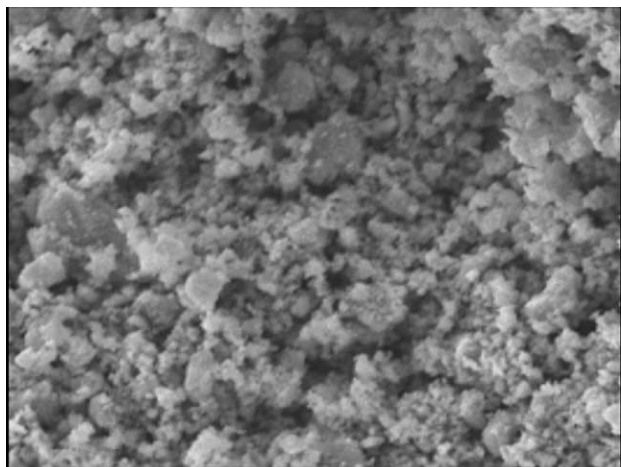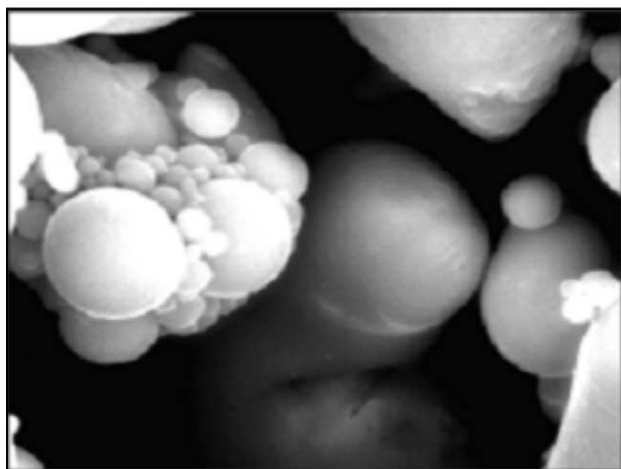

Fig. 1. XRD pattern of as-synthesized SnO_2 powder.

(a)
5 µm

Fig. 4. XRD pattern of Sn:SnO2 (2:1) mixture.

(b)
5 µm

Fig. 2. SEM micrographs of (a) SnO_2 powder; (b) Sn powder.

(a) **Sn:SnO₂ = 1:2**   5 µm

Sn and Li_2O (Eq. (1)), while the broad one extending up to 0.1 V corresponds to the formation of different alloy phases leading finally to $Li_{4.4}Sn$ (Eq. (2)) [4,6,21]. It is clear that the disappearance of the first peak in the subsequent scans is because of the irreversibility of formation of lithia, which
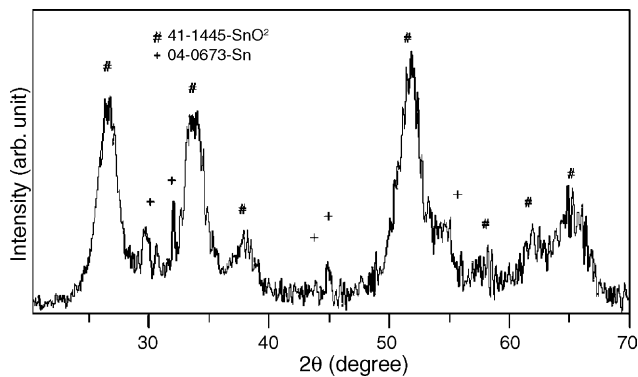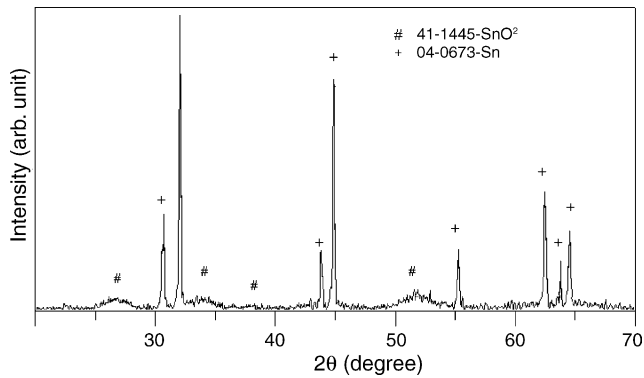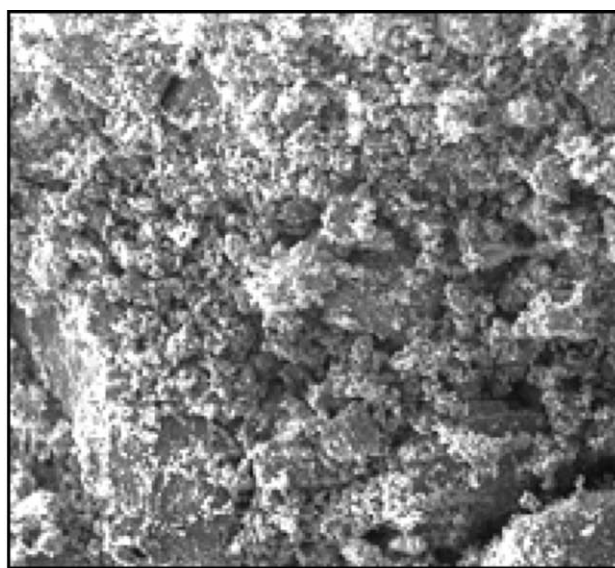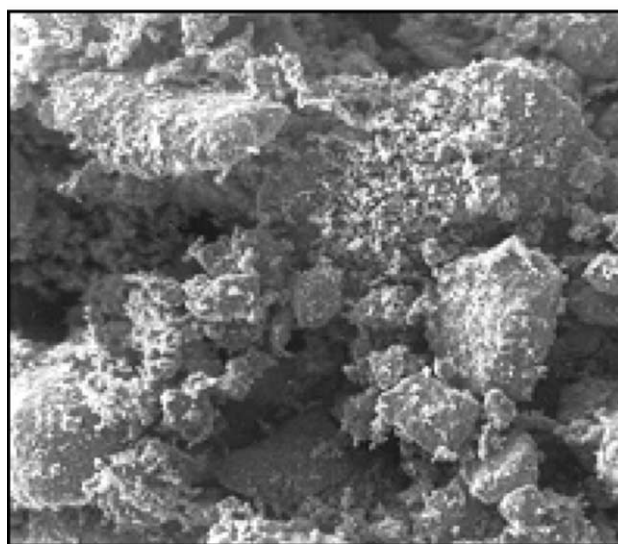

Fig. 3. XRD pattern of Sn:SnO2 (1:2) mixture.

(b) **Sn:SnO₂ = 2:1**   5 µm

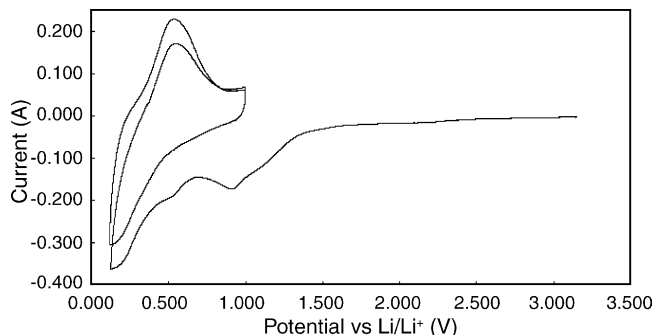Fig. 5. SEM micrographs of Sn–SnO_2 mixtures.

Fig. 6. Cyclic voltammograms of SnO$_2$ electrode.

corresponds to the large irreversible capacity. The absence of well-defined peaks corresponding to the several alloy phases suggests that the necessary rearrangements of the constituent atoms to nucleate the various phases of different crystal structures are slow or are kinetically hindered. The processes being diffusion-controlled manifest as a single-phase transformation. Moreover, the shoulder around 1.25 V, suggesting that the reduction of Sn(IV) to Sn(0) occurs via Sn(II), is in agreement with the earlier observations [6,21–23]. A well-defined broad peak around 0.55 V in the second anodic scan corresponds to the de-lithiation process (Eq. (2)). A single cathodic peak in the subsequent cycles corresponds to the alloying process. The higher currents for the anodic process suggest that the de-alloying process is more facile than the alloying process. Moreover, any segregation of Sn particles can increase the conductivity, leading to higher anodic currents.

3.3. Charge–discharge studies on SnO$_2$ and Sn electrodes

Fig. 7 shows typical charge–discharge curves of SnO$_2$ and Sn electrodes cycled at 0.1 C rate between 1.0 and 0.1 V. It can be seen from the figure that the profile of
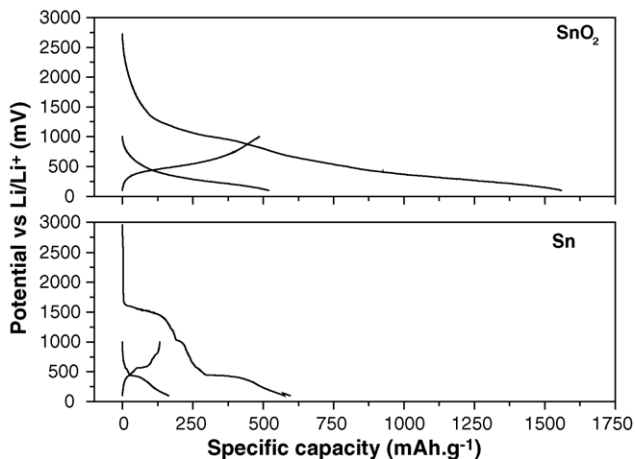
the first insertion in SnO$_2$ reflects a monotonic cathodic process with broad plateaus. It is clear that SnO$_2$ electrodes perform better than Sn electrodes. SnO$_2$ electrodes give a first-cycle irreversible capacity of 1073 mAh g^{-1} and a reversible capacity of 485 mAh g^{-1}, corresponding to a coulombic efficiency of 31%. However, in the subsequent cycles SnO$_2$ exhibit coulombic efficiencies of more than 95%. Over 40 cycles SnO$_2$ electrodes suffer a capacity fade of 1.8 mAh g^{-1} cycle^{-1}, which corresponds to 0.3% of the reversible capacity obtained in the first-cycle.

However, the charge–discharge profiles of Sn appear quite different with several well-defined plateaus. The plateau around 1.0 V is due to reduction of surface oxides, as suggested by the irreversibility of the process. However, the plateau around 1.5 V is not immediately obvious. Predominant plateaus around 0.5 and 0.2 V are attributed to the formation of Li–Sn phases. The de-alloying processes are represented by plateaus between 0.55 and 0.75 V. The good resolution of the plateaus suggests that the alloying reactions proceed in a sequential fashion with several distinct intermediate phases. However, it is difficult to assign these plateaus to individual Li–Sn alloys. The first-cycle reversible capacity of Sn is only 173 mAh g^{-1}, which is just 17% of the theoretical value (994 mAh g^{-1}). Sn electrodes exhibit severe capacity fading upon cycling (Fig. 8), which is a di-
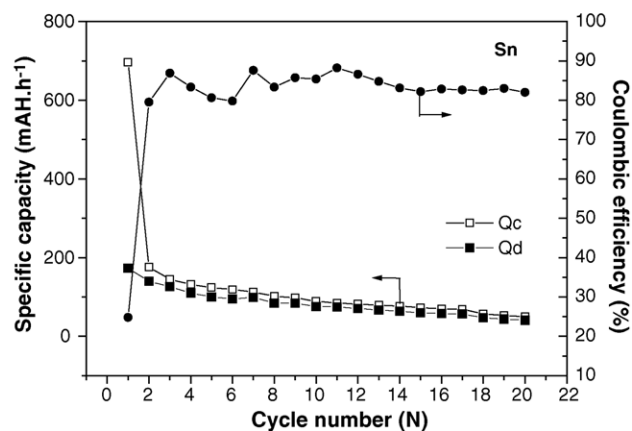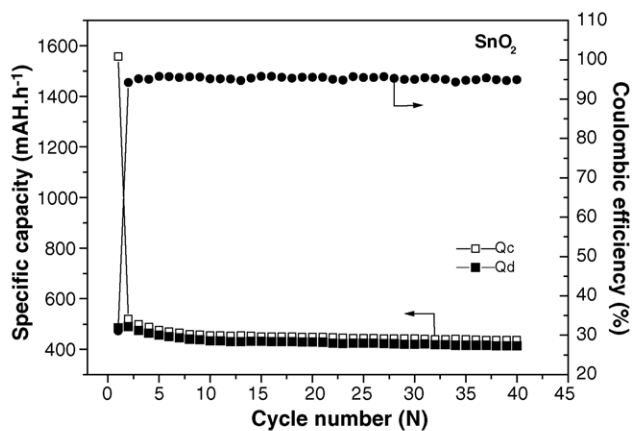

Fig. 8. Comparison of specific capacities of Sn and SnO$_2$ electrodes.

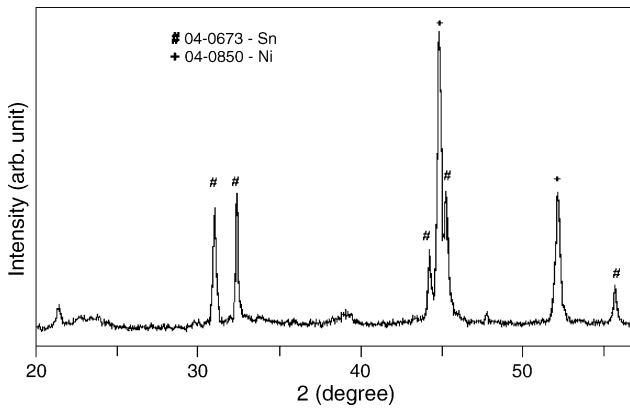Fig. 7. Charge–discharge curves of Sn and SnO$_2$ electrodes.

Fig. 9. Ex-situ XRD pattern of de-inserted SnO_2 electrode.

rect result of the metal undergoing as much as 259% volume expansion in the formation of $Li_{4.4}Sn$. In contrast, the alloying–de-alloying reactions in SnO_2 proceed in a matrix of finely divided Li_2O. The high reversible capacity (485 mAh g^{-1}) and lower capacity fade (0.3%) is due to the resilience provided by the nano-sized lithia particles in the matrix [24]. The ex-situ XRD pattern of the de-inserted electrode (Fig. 9) shows reflections corresponding to Sn and Ni (current collector), which indicate that SnO_2 is completely reduced to Sn. Thus, tin can be cycled efficiently in presence of an inactive matrix. However, the irreversible capacity associated with the formation of the lithia matrix is 1073 mAh g^{-1}.

3.4. Charge–discharge studies on tin–tin oxide mixtures

With a view to increase the reversible capacity and reduce the irreversible capacity and capacity fade upon cycling,

Sn–SnO_2 mixtures, viz., Sn:SnO_2 = 1:2 (SnO_2-rich) and Sn:SnO_2 = 2:1 (Sn-rich) were subjected to charge–discharge studies at a 0.1 C rate between 1.0 and 0.1 V (Fig. 10). The corresponding differential capacity curves are presented in Fig. 11. The SnO_2-rich mixture behaves in a way similar to the SnO_2 electrode in that the plateaus have a smooth transition. Similarly, the charge–discharge profile of the Sn-rich mixture resembles with that of the bare Sn electrode, with sharp transitions.

Fig. 12 illustrates the specific capacities and coulombic efficiencies as a function of the cycle number. It is apparent that the SnO_2-rich mixture performs better than the Sn-rich mixture in that the former has a higher reversible capacity (549 mAh g^{-1}), lower first-cycle irre-
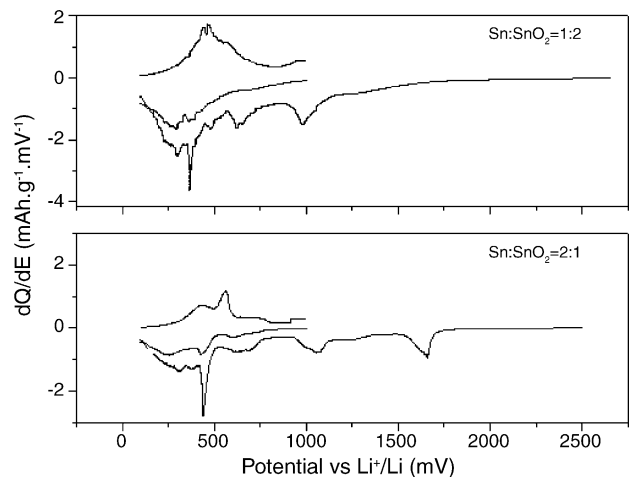

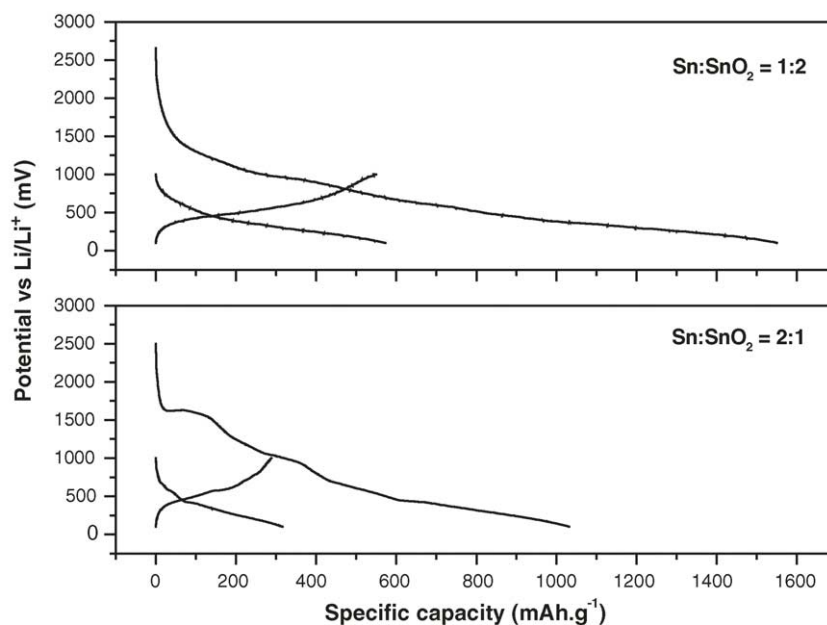Fig. 11. Differential capacity curves for Sn–SnO_2 mixtures.

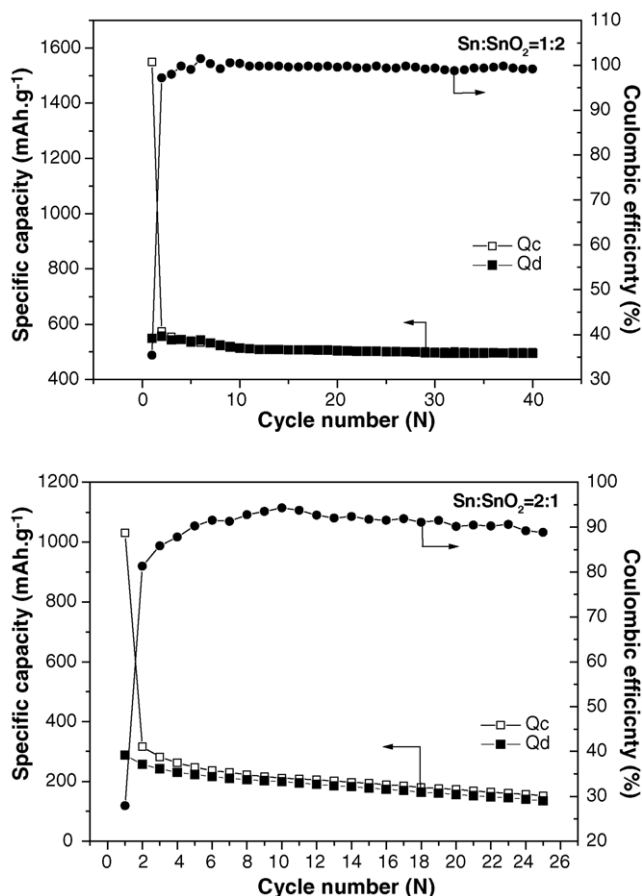Fig. 10. Charge–discharge curves of Sn:SnO_2 mixtures.

Fig. 12. Comparison of specific capacities of Sn–SnO$_2$ mixtures.

versible capacity (1001 mAh g^{-1}) and a higher coulombic efficiency (99%) upon extended cycling (40 cycles). The corresponding values for the Sn-rich mixture are 288 and 743 mAh g^{-1}; and 90%. Furthermore, the SnO$_2$-rich mixture exhibits a low capacity fade (1.4 mAh g^{-1} cycle^{-1}) while in the case of the Sn-rich mixture it is as high as 10 mAh g^{-1} cycle^{-1}.

It is also to be noted that the SnO$_2$-rich mixture outperforms (20% more) the bare SnO$_2$ electrode in terms of higher reversible capacity, lower first-cycle irreversible capacity and higher coulombic efficiency. As expected, an increase in the reversible capacity (by 13%) and a decrease in the first-cycle irreversible capacity (by 7%) are obtained. The better performance of the SnO$_2$-rich mixture is attributed to the limited oxygen content in the mixture, which consumes less lithium for the irreversible formation of Li$_2$O, thereby offering a low irreversible capacity. This is contrary to expectations with a metal-rich mixture. The lower capacity realized for the Sn-rich mixture must be attributed to the fact that the alloying metal particles are larger than the nanoparticulate tin generated by the reduction of SnO$_2$. Additionally, the Li$_2$O matrix generated in the case of the SnO$_2$-rich mixture provides a sufficiently facile environment for the dispersion of the Sn particulates and lithium ion diffusion in it,

resulting in a greater utilization of the active material phase. Clearly, the amount of Li$_2$O formed in the SnO$_2$-rich electrode is sufficient to prevent agglomeration of Sn or Sn–Li alloy particles into large and less efficient particles. Morimoto et al. [25] obtained similar results with mechanically milled SnO–B$_2$O$_3$–P$_2$O$_5$ composites with and without Li$_2$O. Anodes containing Li$_2$O delivered capacities slightly higher than those without Li$_2$O, suggesting that the addition of Li$_2$O accelerated lithium extraction from the amorphous anode material. It is believed that the diffusion of lithium into the amorphous material with Li$_2$O must be faster and/or that the morphology of the particle in the two cases must be different.

The appearance of well-resolved peaks in the differential capacity curve of the Sn-rich mixture indicates the formation of ordered intermediate alloy phases at around 0.5 V. The associated volume changes hinder the diffusion of lithium into the interior of the resulting segregated active phases. On the other hand, the appearance of smooth peaks in the differential capacity curves of the SnO$_2$-rich mixture indicates that the Li$_2$O matrix formed accelerates lithium extraction from the amorphous anode material [25]. Thus, it is evident that Sn–SnO$_2$ mixtures can be choice-materials for use as anodes in lithium-ion battery application.

4. Conclusions

An attempt is made to reduce the high irreversible capacity of SnO$_2$-based electrodes by use of a novel approach involving Sn and SnO$_2$ mixtures. Two compositions, viz., Sn:SnO$_2$ = 1:2 and 2:1, were investigated. The 1:2 Sn:SnO$_2$ mixture exhibited a higher specific capacity of 549 mAh g^{-1} (13% higher than that for the bare SnO$_2$) with a lower irreversible capacity (7% lower than that for the bare SnO$_2$) and a capacity fade of 1.4 mAh g^{-1} cycle^{-1} upon extended cycling. The SnO$_2$-rich mixture also exhibited a higher coulombic efficiency (99%) over 40 cycles than did SnO$_2$ and the Sn-rich mixture. It appears that a matrix in which tin can be distributed without agglomeration is essential for realizing tin oxide anodes with high cyclability.

References

[1] Y. Idota, M. Mishima, M. Miyaki, T. Kubota, T. Miyasaka, Eur. Pat. Appl. 65140 A194116643.1 (1994).

[2] K. Tahara, H. Ishikawa, F. Iwasaki, S. Yahagi, A. Sakkata, T. Sakai, Eur. Pat. Appl. 93111938.2 (1993).

[3] Y. Idota, T. Kubota, A. Matsufuji, Y. Maekawa, T. Miyasaka, Science 276 (1997) 1395.

[4] I.A. Courtney, J.R. Dahn, J. Electrochem. Soc. 144 (1997) 2045.

[5] I.A. Courtney, J.R. Dahn, J. Electrochem. Soc. 144 (1997) 2943.

[6] T. Brousse, R. Retoux, U. Herterich, P.M. Schleich, J. Electrochem. Soc. 145 (1998) 1.

[7] J. Yang, M. Winter, J.O. Besenhard, Solid State Ionics 90 (1996) 281.

[8] C.J. Wen, R.A. Huggins, J. Electrochem. Soc. 128 (1980) 1181.

[9] T. Arai, J. Phys. Soc. Jpn. 15 (1960) 916.

[10] B. Orel, U. Lavrencic-Stangar, Z.C. Orel, P. Bulkovec, M. Kosec, J. Non-Cryst. Solids 167 (1994) 272.

[11] Y. Takahashi, Y. Wada, J. Electrochem. Soc. 137 (1990) 267.

[12] S.R. Davis, A.V. Chadwick, J.D. Wright, J. Mater. Chem. 8 (1998) 2065.

[13] C.V. Santilli, S.H. Pulcinelli, G.E.S. Brito, V. Briosis, J. Phys. Chem. B103 (1999) 2660.

[14] R.C. Mehrotra, J. Non-Cryst. Solids 121 (1990) 1.

[15] D. Wand, S. Wen, J. Chen, S. Zhang, F. Li, Phys. Rev. B49 (1994) 14282.

[16] R.D. Tarey, T.A. Raju, Thin Solid Films 128 (1995) 181.

[17] T. Minami, H. Nanto, S. Takata, Jpn. J. Appl. Phys. 27 (1988) 287.

[18] V. Schlosser, G. Wind, Proceedings of the 8th EC Photovoltaic Solar Energy Conference, Florence, Italy, 1998, p. 998.

[19] J. Lee, S. Park, J. Am. Ceram. Soc. 76 (1993) 777.

[20] H. Klug, L. Alexander, X-Ray Diffraction Procedure, Wiley, New York, 1962, pp. 125.

[21] S. Panero, G. Savo, B. Scrosati, Electrochem. Solid-State Lett. 2 (1999) 365.

[22] J. Isidorsson, C.G. Granqvist, L. Haggstrom, E. Nordstrom, J. Appl. Phys. 80 (1996) 2367.

[23] N. Li, C.R. Martin, J. Electrochem. Soc. 148 (2001) 164.

[24] M. Winter, J.O. Besenhard, Electrochim. Acta 45 (1999) 31.

[25] H. Morimoto, M. Nakai, M. Tatsumisago, T. Minami, J. Electrochem. Soc. 146 (1999) 3970.